Heart Surgery Forum 2023; 26(6): E740–E754
doi: 10.59958/hsf.6809

Article

Identification of Anesthetic-Induced Cardiovascular Biomarkers in Off-Pump Coronary Artery Bypass Grafting Surgery Using Weighted Gene Co-Expression Network Analysis and Machine Learning

Jinxiu Hou[1], Jing Li[2,*]

[1]School of Anesthesiology, Weifang Medical University, 261053 Weifang, Shandong, China
[2]Department of Gastroenterology, Weifang People's Hospital, 261041 Weifang, Shandong, China
*Correspondence: ljing1101@126.com (Jing Li)

Submitted: 10 September 2023 Revised: 29 October 2023 Accepted: 1 November 2023 Published: 18 December 2023

Abstract

Background: This study aimed to select anesthesia-induced zinc finger protein-related gene biomarkers that predict cardiovascular function during off-pump coronary artery bypass grafting (OPCABG). **Methods**: Gene expression data from GSE4386 included 20 post-anesthesia and 20 pre-anesthesia atrial tissue samples. Zinc finger protein-related genes (ZFPRGs) were searched in the UniProt database and anesthesia-induced differentially expressed genes (DEGs) were identified Weighted gene co-expression network analysis (WGCNA) was used to screen hub genes, and three machine learning algorithms were used to further screen for cardiovascular biomarkers. Diagnostic accuracy was evaluated using a nomogram model. Gene set enrichment analysis was used to analyze the pathways enriched by the biomarkers. A microRNA (miRNA)-mRNA-transcription factor (TF) regulatory network was established to explore the potential regulatory mechanisms of these biomarkers. Disease-related drugs were predicted using the Comparative Toxicogenomics Database (CTD). **Results**: A total of 1102 cardioprotection-related DEGs were selected between the pre- and post-anesthesia groups. Additionally, 1095 hub genes were obtained based on WGCNA, and 2274 ZFPRGs were downloaded from the UniProt database. After Venn analysis and machine learning, *ZNF420*, *RNF135*, and *BNC2* were selected as cardioprotection-related zinc finger biomarkers during OPCABG. Receiver operating characteristic (ROC) curves and nomogram models confirmed the diagnostic value and accuracy of the three cardioprotective biomarkers. Pathway enrichment analysis revealed that *ZNF420* is involved in the cell cycle and the tricarboxylic acid cycle. *RNF135* and *BNC2* were enriched in the oxidative phosphorylation pathway. In the constructed miRNA-mRNA-TF network, miR-182-5p and miR-16-5p simultaneously regulated three cardioprotective biomarkers. **Conclusion**: Three cardioprotection-related zinc finger protein biomarkers (*ZNF420*, *RNF135*, and *BNC2*) were identified using OPCABG samples.

Keywords

biomarker; machine learning; off-pump coronary artery bypass grafting; weighted gene co-expression network analysis

Introduction

Off-pump coronary artery bypass grafting (OPCABG) is an innovative procedure in cardiac surgery that has emerged in recent years, avoiding systemic inflammation, coagulation dysfunction, myocardial damage, multiple organ dysfunction, and other after-effects of extracorporeal circulation [1,2]. OPCABG also reduces the risk of neurological complications compared to extracorporeal coronary artery bypass grafting [3,4]. OPCABG is a myocardial revascularization program that improves hemodynamic parameters and reduces sympathetic nerve pressure [5]. After OPCABG, the incidences of post-operative mortality and stroke in older individuals are extremely low, suggesting that this surgery is safe for coronary artery disease in this population [6]. OPCABG accounts for 15–30% of all cases of coronary artery bypass grafting (CABG) and presents with excellent short-term outcomes [7]. Although OPCABG has become the gold standard treatment for multivessel coronary artery disease, it is associated with irreversible myocardial injury [8]. Thus, reducing cardiac damage and improving post-ischemic recovery remain to be achieved.

During surgery, patients must be anesthetized [9]. Common anesthetic methods include inhalation and intravenous administration. Anesthesia with sevoflurane reduces the release of cardiac biomarkers [10]. Total intravenous anesthesia with propofol can be induced quickly and stably during recovery, with few side effects. They are harmless and more effective than hypnotic drugs [11]. In addition, it can reduce myocardial reperfusion injury in patients undergoing OPCABG [12]. Growing evidence suggests that sevoflurane and propofol have cardioprotective effects [13]. Moreover, anesthetic gas administration can

modulate the expression of target genes involved in myocardial substrate metabolism and protect cardiac function [14]. Thus, anesthetic-induced cardiac biomarkers play a key role in cardiac protection.

Zinc finger proteins are among the most abundant families of proteins. They can interact with ribonucleic acid (RNA), deoxyribonucleic acid (DNA), and poly-ADP-ribose, and are involved in the regulation of many cellular processes [15]. Zinc finger proteins are associated with cardiovascular diseases [16,17]. Meng *et al*. [18] implicated the zinc finger transcription factor ZFP580 in the cardioprotective effects of intermittent high-altitude hypoxia against myocardial ischemia-reperfusion injury. However, whether zinc finger proteins can serve as anesthetic-induced cardioprotective biomarkers remains unclear.

In this study, we selected anesthesia-induced cardioprotection-related zinc finger protein biomarkers. Weighted gene co-expression network analysis (WGCNA) was used to screen hub genes, and three machine learning algorithms were applied to further screen biomarkers. Additionally, a miRNA-mRNA transcription factor (TF) regulatory network was established to explore the potential regulatory mechanisms of the biomarkers. The diagnostic accuracy of biomarkers was evaluated using a nomogram model. Our results may improve our understanding of the mechanisms underlying the cardioprotective effects of anesthesia during OPCABG.

Materials and Methods

Data Sources

The gene expression profile dataset GSE4386, which contained samples associated with OPCABG using the anesthetic gas sevoflurane and intravenous anesthetic propofol, was downloaded from the Gene Expression Omnibus (GEO) database and used in this study. In a prospective randomized trial with ethics committee approval, male patients with three-vessel coronary artery disease aged 50–80 years were included and allocated to receive either sevoflurane (n = 10) or propofol (n = 10) [1]. For each patient, two atrial samples (immediately after chest opening and shortly before chest closing) were collected. The former reflected the background expression profile before exposure to anesthesia (control group), whereas the latter mirrored the gene response to anesthesia (anesthesia group). The dataset was developed using the GPL570 [HG-U133_Plus_2] Affymetrix Human Genome U133 Plus 2.0 Array annotation platform.

Zinc finger protein-related genes (ZFPRGs) were searched from the UniProt database with "zinc finger protein" as the keywords, and the organism parameter was set to *Homo sapiens*.

Differentially Expressed Genes (DEGs) Screening

Series matrix files were downloaded and log2 transformed. The annotation information of gene expression data was downloaded based on the GPL570 [HG-U133_Plus_2] Affymetrix Human Genome U133 Plus 2.0. The probes were mapped to gene symbols, and probes with no match to the gene symbols were removed. For different probes mapped to the same gene, the mean value of different probes was calculated as the final expression value of the given gene. The DEGs between the anesthesia (propofol or sevoflurane) and control groups were analyzed using the R package limma 3.42.2 (Bioconductor, Dana-Farber Cancer Institute, Boston, Massachusetts, USA). The screening conditions for DEGs were $p < 0.05$ and $|\log2FC| > 0.5$. R packages ggplot2 3.3.2 and pheatmap 0.7.7 were used to visualize the results. The online tool jvenn was used to determine the intersection of the DEGs caused by propofol and sevoflurane.

WGCNA

To filter the potential genes associated with anesthesia, a weighted gene co-expression network was constructed based on the expression matrix of the DEGs. First, the samples were clustered, and outlier samples were eliminated. A soft threshold was then determined to ensure that the interactions between genes conformed to a scale-free distribution. The recommended optimal power value in the WGCNA package (1.70.3) (University of California, Berkeley, CA, USA) [19] was 14. Subsequently, a co-representation matrix was constructed. Briefly, the adjacency between genes was calculated, the similarity between genes was calculated according to adjacency, and the divergence coefficient between genes was derived to obtain a systematic clustering tree. The minimum number of genes in each module was set based on the dynamic tree-cutting algorithm. To screen out the key modules that were highly correlated with anesthesia, the modules that were equally correlated with the sample traits were screened as key modules ($p < 0.05$; correlation coefficients >0.3). Genes in key models were considered hub genes.

Differentially Expressed (DE) ZFPRG Screening

Based on the 2274 ZFPRGs obtained from the UniProt database, common DEGs and hub genes obtained from WGCNA and the intersection genes (DE ZFPRGs) were screened using jvenn.

Functional Analysis of DE ZFPRGs

To dissect the potential functions related to DEZFPRGs, Gene ontology (GO) functional enrichment analyses were conducted using R ClusterProfiler 3.14.3 (developed by Guangchuang Yu, Key Laboratory of Functional Protein

Research of Guangdong Higher Education Institutes, Jinan university, Guangzhou, China) [20]. The GO database was constructed using three independent categories: biological processes (BP), cellular components (CC), and molecular functions (MF). GO terms with $p < 0.05$ were considered significant, and the top 10 enrichment results in each category were visualized using ggplot 2 3.3.2 (developed by Hadley Wickham, University of Auckland, Auckland, New Zealand).

Correlation Analysis of DE ZFPRGs

Combined with the anesthesia grouping information of the samples, the correlation between genes was calculated using the Pearson method, and the corresponding correlation coefficient and *p* value were obtained. The R package ggplot2 3.3.2 was used to visualize the correlation results.

Biomarker Screening by Machine Learning

Machine learning algorithms are increasingly used for biomarker identification. In this study, three machine learning algorithms (Least Absolute Shrinkage and Selection Operator (LASSO) regression analysis, support vector machine (SVM), and random forest) were used to screen biomarkers.

(1) Using the expression values of DE ZFPRGs in samples from the dataset GSE4386, combined with sample grouping, LASSO regression prediction sample classification was constructed. To reduce the characteristic dimension, the R glmnet 4.0-2 (developed by Trecor Hastie, Stanford university, San Francisco, CA, USA) [21] was used with parameters family = "binomial", type. measure = "class", nfold = 10 to perform LASSO logistic regression. A 10-fold cross-validation was used to calculate the error rate for different characteristics. Feature genes were selected when the criteria for lambda min were used.

(2) The SVM algorithm in R E1071 1.7-9 (R Development core team, University of Auckland, Auckland, New Zealand) [22] embedding 5-fold cross-validation was used to sort the DE ZFPRGs. A recursive feature elimination method was used to obtain the importance and importance ranking of each gene, and the error rate and accuracy of each iteration combination were obtained. The combination with the lowest error rate was selected, and the corresponding genes were selected as characteristic genes.

(3) The random forest method in R package randomForest 3.36.0 (University of California, Berkeley, CA, USA) was used to screen characteristic genes based on the 24 DE ZFPRGs, and the obtained genes were ranked by two methods: mean decrease accuracy and mean decrease gini. The top 10 genes were selected and visualized in lollipop charts.

Finally, the characteristic genes screened by the three algorithms were intersected using the R package UpsetR 1.4.0 (Jake R. Conway, Boston, MA, USA). The genes in the intersections were considered biomarkers.

Diagnostic Value, Correlation, and Regulatory Network Analyses of Biomarkers

To assess the diagnostic value of the biomarkers, receiver operating characteristic (ROC) curve analysis was performed for each biomarker using the R package pROC 1.12.1 (Robin X, BioMed Central Ltd., Geneva, Switzerland). Additionally, the expression values of biomarkers were extracted from the dataset GSE4386 and plotted using the Wilcoxon test method in ggplot2 3.3.2, combined with the sample grouping information of the dataset.

The expression levels of biomarkers were obtained from the dataset, and the correlation between biomarkers was calculated using the Pearson method in the anesthesia samples of the dataset combined with the anesthesia grouping of samples.

Additionally, protein-protein interaction (PPI) regulatory network analysis of biomarkers was performed using the GeneMANIA database to predict co-localization, shared protein domains, co-expression, and pathways.

Nomogram Construction

A nomogram model was constructed to verify the diagnostic value of the selected biomarkers in cardiovascular diseases. Based on the biomarkers obtained above, RMS 6.4-1 (Harrell Jr, Duke University, Durham, NC, USA) [23] was used to construct the nomogram prediction model, and calibration and ROC curves were used to evaluate the predictive ability of the nomogram.

Gene Set Enrichment Analysis (GSEA)

To understand the biological value of a single biomarker, GSEA was performed for each biomarker using the GSEA software 4.0.3 (Fred Hutchinson Cancer Research Center, Seattle, WA, USA). The "c2.cp.kegg.v7.5.1.symbols.gmt", and "c5.go.bp.v7.5.1. symbols.gmt" were used as reference gene sets for KEGG and GO BP, respectively. The thresholds of significance were $|NES| > 1$ and NOM $p < 0.05$.

Regulatory Network Analysis

MiRNAs and TFs play crucial roles in the regulation of gene expression. To explore the regulatory mechanism of gene biomarker expression, a miRNA-mRNA-TF regulatory network was constructed. The miRNA prediction of biomarkers was performed using the NetworkAnalyst database (parameters: Specify organism: *H. sapiens*, Gene-miRNA interaction database: TarBase v8.0). Addition-

Table 1. List of primer sequences.

Symbol	Sequences
BNC2	Forward 5′-CTTTTCAAAGTTGCTGAAATAAAA-3′ Reverse 5′-TTGCATTTAATGGCCTCAGA-3′
ZNF420	Forward 5′-AGACAATATCCCGCTGTACGAATATCCTGTAGT-3′ Reverse 5′-ATTCCCCGAGATAAATCCGATTATGAAGCC-3′
RNF135	Forward 5′-CTGCGGAAGAACACGCTACT-3′ Reverse 5′-GCTCAGTTCGTTGTCTGGTCC-3′
GAPDH	Forward 5′-CCACTCCTCCACCTTTGAC-3′ Reverse 5′-ACCCTGTTGCTGTAGCCA-3′

ally, TF prediction was performed using the NetworkAnalyst database and the parameters were Specify organism: *H. sapiens*, TF-gene interaction database: ENCODE. With the obtained miRNA-mRNA and mRNA-TF relation pairs, the miRNAs and TFs that regulated the same mRNA were selected to establish the miRNA-mRNA-TF regulatory network using Cytoscape 3.6.1 (University of California, San Diego, Chile).

Drug Prediction Using Biomarkers

Disease-related drugs were predicted by using each biomarker as a keyword in the Comparative Toxicogenomics Database (CTD) database. Cytoscape (version 3.6.1) was used to visualize the drug-target relationship network.

Validation of the Expression of Biomarkers by Real-time PCR Analysis

Five patients with multi-vessel coronary artery disease who underwent OPCABG at our hospital were enrolled. This study was approved by the Ethics Committee and conducted in compliance with the Declaration of Helsinki. Five pairs of cardiac tissues were collected before (immediately after chest opening) and after anesthesia (shortly before chest closing). The tissue samples were stored at –80 °C for further use.

For Reverse transcription quantitative polymerase chain reaction (RT-qPCR) analysis, total RNA was extracted from cardiac tissues using the TRIzol reagent. cDNA was obtained from RNA samples (1 µg) based on a cDNA synthesis kit (Thermo Fisher Scientific, Waltham, MA, USA). Real-time PCR was performed using a Bio-Rad real-time PCR system. The primer sequences used for ZNF420, BNC2, and RNF135 are summarized in Table 1. The reaction conditions were 95 °C for 2 min, followed by 35 cycles of 95 °C for 10 s and 65 °C for 15 s. Gene expression was analyzed using the $2^{-\Delta\Delta Ct}$ method relative to GAPDH.

Statistical Analysis

Experiments were conducted in triplicate and the continuous variables are displayed as mean ± SD. Data were compared between groups using an unpaired *t*-test. Differences with a $p < 0.05$ was considered significant.

Results

DEG Identification

Based on the cutoff value of $p < 0.05$ and $|\log2FC| > 0.5$, a total of 1309 DEGs were obtained in the propofol *vs.* control groups, including 539 upregulated and 770 downregulated; 1959 DEGs were obtained in the sevoflurane *vs.* control groups, including 875 upregulated and 1084 downregulated. A volcano map was used to display the distribution of DEGs (Fig. 1A). The heatmaps of the two groups of DEGs are shown in Fig. 1B. A total of 1102 common DEGs were identified between the two groups (Fig. 1C).

Hub Gene Selection Using WGCNA

The overall correlation between data samples is shown in Fig. 2A. The clustering of the samples in the dataset was good; therefore, no samples were excluded. Subsequently, the sample traits were sorted and added to the clustering diagram to construct a heat map of sample clustering and clinical traits (Fig. 2B). The power value was 14 and the R^2 was approximately 0.85 (Fig. 2C), indicating that the network was closer to a scale-free distribution. Simultaneously, the mean value of the adjacency function gradually approached zero, showing a gradual trend (Fig. 2D). Then, 21 modules were selected using a system clustering tree (Fig. 2E). A heatmap of the correlation between the modules and clinical traits is shown in Fig. 2F. The dark red, magenta, green-yellow, and turquoise modules were positively correlated with propofol, and the yellow module was negatively correlated with the anesthetic. The black and pink modules positively correlated with sevoflurane, whereas the yellow module negatively correlated with the anesthetic. Finally,

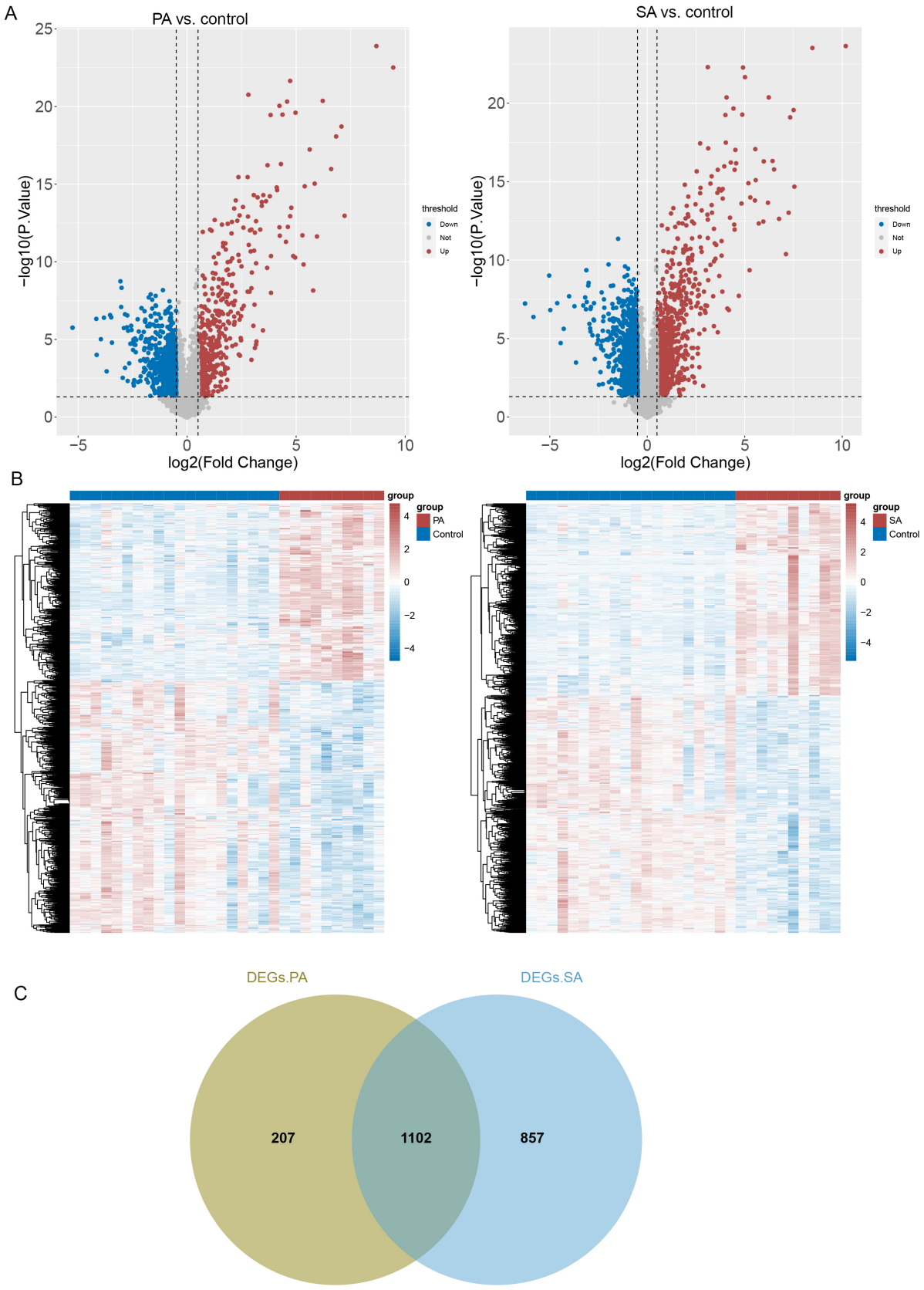

Fig. 1. Differentially expressed genes (DEGs) identification. (A) Volcano maps of DEGs in PA (propofol anesthesia) *vs*. control and SA (sevoflurane anesthesia) *vs*. control. (B) Heatmaps of DEGs in PA *vs*. control and SA *vs*. control. (C) Venn diagram of DEGs in PA *vs*. control and SA *vs*. control.

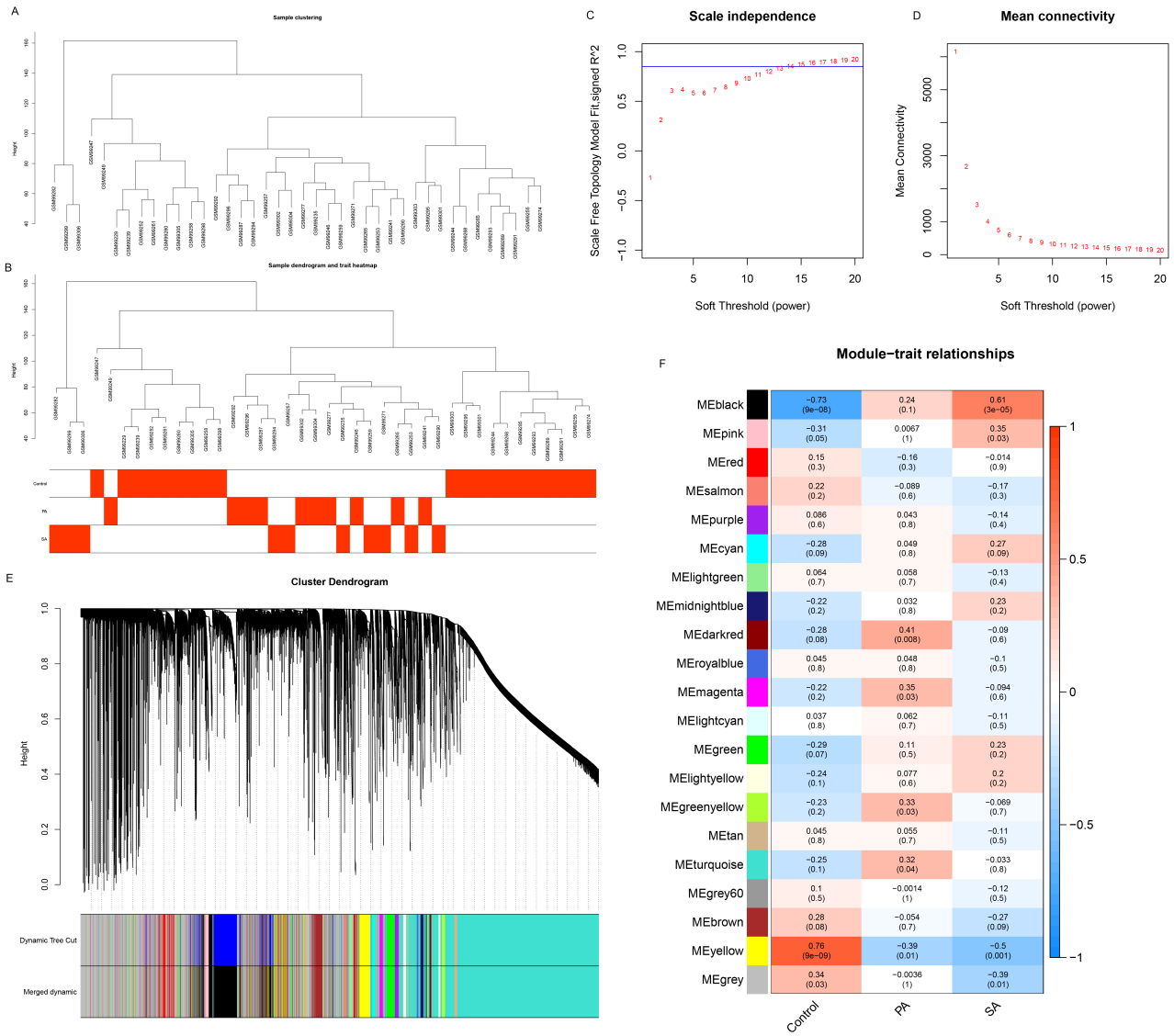

Fig. 2. Hub genes selection by Weighted gene co-expression network analysis (WGCNA). (A) The overall correlation of the data sample. (B) The heatmap of sample clustering and clinical traits. (C,D) Scale-free soft threshold distribution. (E) Module clustering tree. (F) Heatmap of correlation between modules and clinical traits.

the yellow module that correlated with the sample traits was selected as the key module, which included 1095 hub genes.

DE ZFPRG Screening and Functional Analysis

A total of 2274 ZFPRGs were obtained from the UniProt database after removing duplicates. Based on 2274 ZFPRGs, 1102 common DEGs, and 1095 hub genes, 24 intersection genes were identified (Fig. 3A). According to the significance threshold ($p < 0.05$), 143 GO BP (such as regulation of transcription, DNA-template, and regulation of RNA biosynthetic process), eight GO CC (such as the cytoplasmic side of lysosomal membrane and endoplasmic reticulum tubular network membrane), and 19 GO MF (such as metal ion binding, cation binding, and zinc ion binding) were obtained. The top 10 results are shown in Fig. 3B–D. The expression levels of the intersecting genes were obtained from the dataset GSE4386. Combined with the anesthesia grouping information of the samples, the correlation between the intersecting genes in the anesthesia samples was calculated. As shown in Fig. 3E, there was a strong positive correlation between *ATL1* and *BNC1*.

Biomarker Screening Using Machine Learning

Based on the LASSO regression analysis, the minimum error rate was obtained when lambda.min was 0.0996, and four feature genes (*ZNF420*, *RNF135*, *BNC2*, and *BNC1*) were selected (Fig. 4A). Using an SVM, nine characteristic genes (*ZNF420*, *RNF135*, *ATL1*, *ZNF813*, *OSR1*, *BNC2*, *ZNF518A*, *ZBTB8A*, and *PRDM6*) were identified (Fig. 4B). In the random forest model, after ranking the vari-

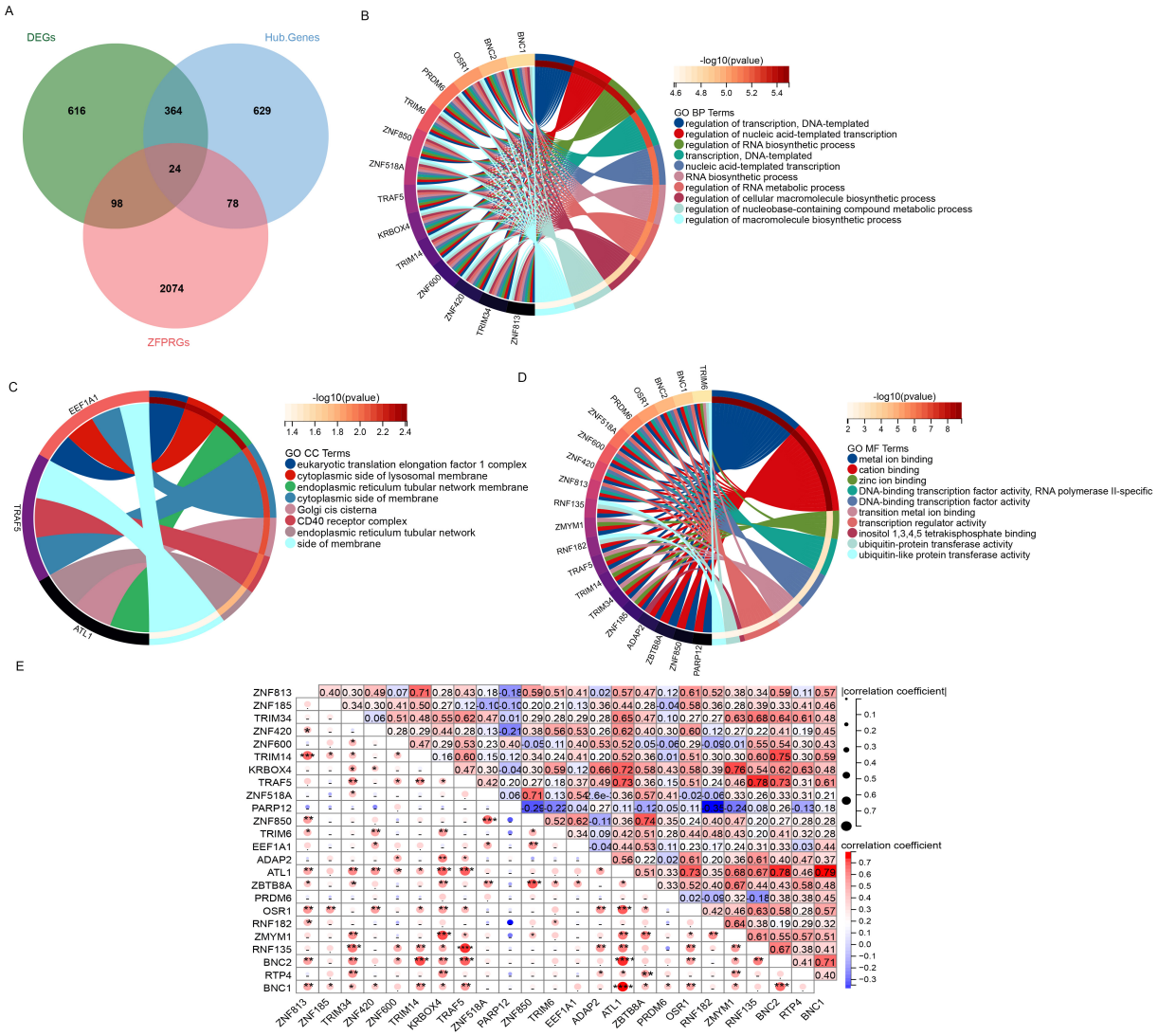

Fig. 3. Differentially expressed ZFPRGs screening, function analysis and correlation analysis. (A) Venn diagram of 2274 ZFPRGs, 1102 common DEGs, and 1095 hub genes. (B–D) Gene ontology (GO) biological processes (B), cellular components (C) and molecular functions (D) enriched by differentially expressed ZFPRGs. (E) The correlation between differentially expressed ZFPRGs in the anesthesia samples. "*, **, *** and ****" indicate $p < 0.05$, <0.01, <0.001 and <0.0001, respectively.

ables (genes) by mean decrease accuracy, the top 10 genes (*OSR1*, *RNF135*, *RTP4*, *ZNF518A*, *ZNF420*, *BNC2*, *BNC1*, *PRDM6*, *ZNF813*, and *ADAP2*) were selected to plot the lollipop chart (Fig. 4C). The genes screened by the three machine learning algorithms were intersected using the R package UpsetR and three biomarkers (*ZNF420*, *RNF135*, and *BNC2*) were identified (Fig. 4D).

Diagnostic Value, Correlation, and Regulatory Network Analyses of Biomarkers

ROC analysis of the three biomarkers showed that the area under curve (AUC) values of all biomarkers were >0.85, indicating that the biomarkers had the diagnostic ability to distinguish between the two groups (Fig. 5A). Additionally, the expression levels of the three biomarkers differed significantly between the control and anesthesia groups ($p < 0.0001$) (Fig. 5B). Pearson correlation analysis revealed a strong positive correlation between *RNF135* and *BNC2* (Fig. 5C).

A gene-gene functional interaction network of the three biomarker genes was constructed and other 20 correlated genes (*DDX58*, *NLRX1*, and *NLRC5*) were predicted based on the GeneMANIA database. The proteins in the network were associated with functions of regulation of type I interferon production, type I interferon production, negative regulation of cytokine production, and others (Fig. 5D).

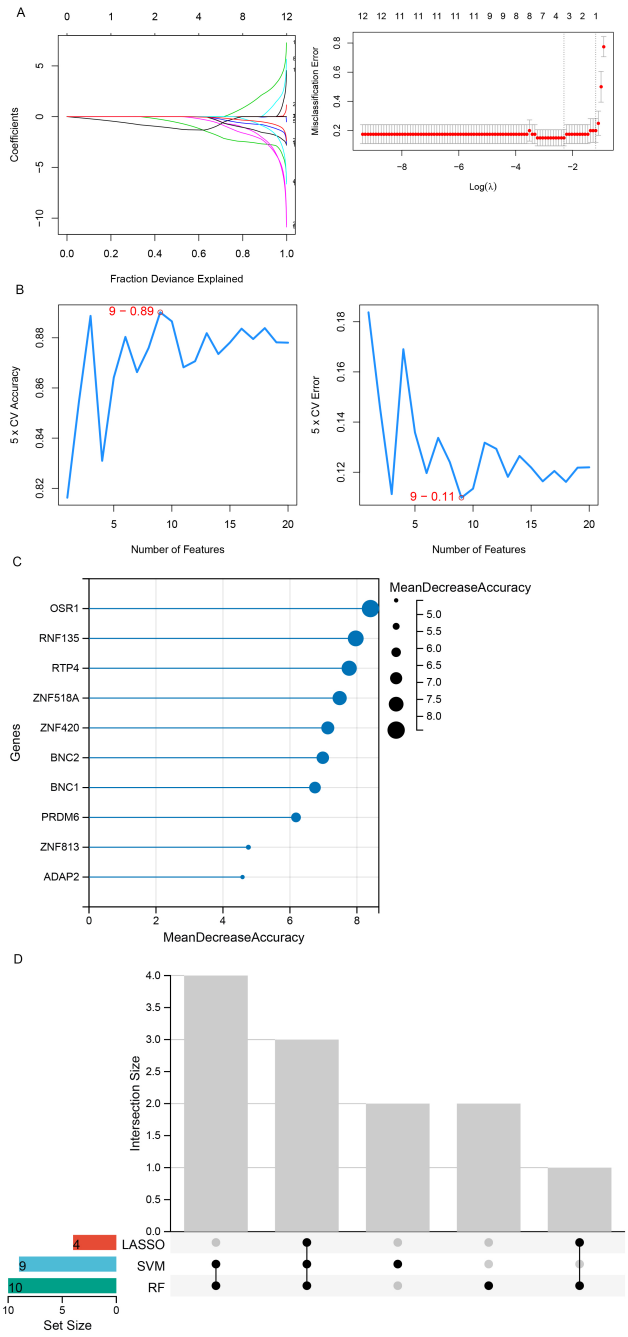

Fig. 4. Biomarkers screening by machine learning. (A–C) Characteristic genes screening by Least Absolute Shrinkage and Selection Operator (LASSO) regression analysis (A), support vector machine (SVM) (B) and random forest model (C). Venn diagram of the genes screened by the three machine learning algorithms (D).

Nomogram Construction

Based on the three biomarkers, the sample grouping information, and marker expression levels, a nomogram model of the markers was constructed (Fig. 6A). A calibration curve revealed that the error between the actual anesthesia risk and the predicted risk was small, indicating that the nomogram model had a high prediction accuracy for sample anesthesia (Fig. 6B). Additionally, the AUC of the ROC curve for the nomogram model was 0.978, further suggesting its effectiveness (Fig. 6C).

GSEA

GSEA was performed to explore the functions of the biomarkers (Fig. 6D). *ZNF420* is associated with functions related to morphogenesis, cardiac myofibril assembly, and centriole assembly. Additionally, it is involved in the cell cycle, tricarboxylic acid (TCA) cycle, and dilated cardiomyopathy pathways. *RNF135* is enriched in antigen processing and the presentation of exogenous antigen-related functions and pathways of allograft rejection, oxidative phosphorylation, and neuroactive ligand-receptor interaction. *BNC2* is also enriched in antigen processing and presentation of exogenous antigen-related functions. Additionally, it is involved in the cell adhesion molecule cam pathways, oxidative phosphorylation, and olfactory transduction.

MiRNA-mRNA-TF Regulatory Network Construction

Using the Network Analyst database, 67 miRNA-mRNA and 25 mRNA-TF pairs were predicted. Based on these miRNA-mRNA and mRNA-TF pairs, miRNAs and TFs regulated by the same mRNA were screened. Finally, 425 miRNA-mRNA-TF regulatory pairs were identified, including 58 miRNAs, 3 mRNAs, and 24 TFs. This network is shown in Fig. 7A. miR-182-5p and miR-16-5p simultaneously regulated these three biomarkers. Both *ZNF420* and *RNF135* were regulated by WT1, and *ZNF420* and *BNC2* were regulated by MAZ.

Drug Prediction Using Biomarkers

Drugs related to each biomarker were searched in the CTD database. Ten drugs were obtained: tretinoin, cisplatin, and estradiol for *BNC2*; amiodarone and resveratrol for *ZNF420*; and tretinoin, cisplatin, and bisphenol A for *RNF135* (Fig. 7B).

Gene Expression Validation in Clinical Samples

The expression of ZNF420, BNC2, and RNF135 was determined in cardiac tissues using RT-qPCR analysis. The tissues obtained before anesthesia were considered the control group, and the tissues obtained after anesthesia were considered the anesthesia group. The results showed that *ZNF420*, *BNC2*, and *RNF135* were all significantly downregulated by anesthesia in comparison to controls (all $p < 0.05$, Fig. 8), which is consistent with the bioinformatics analysis results.

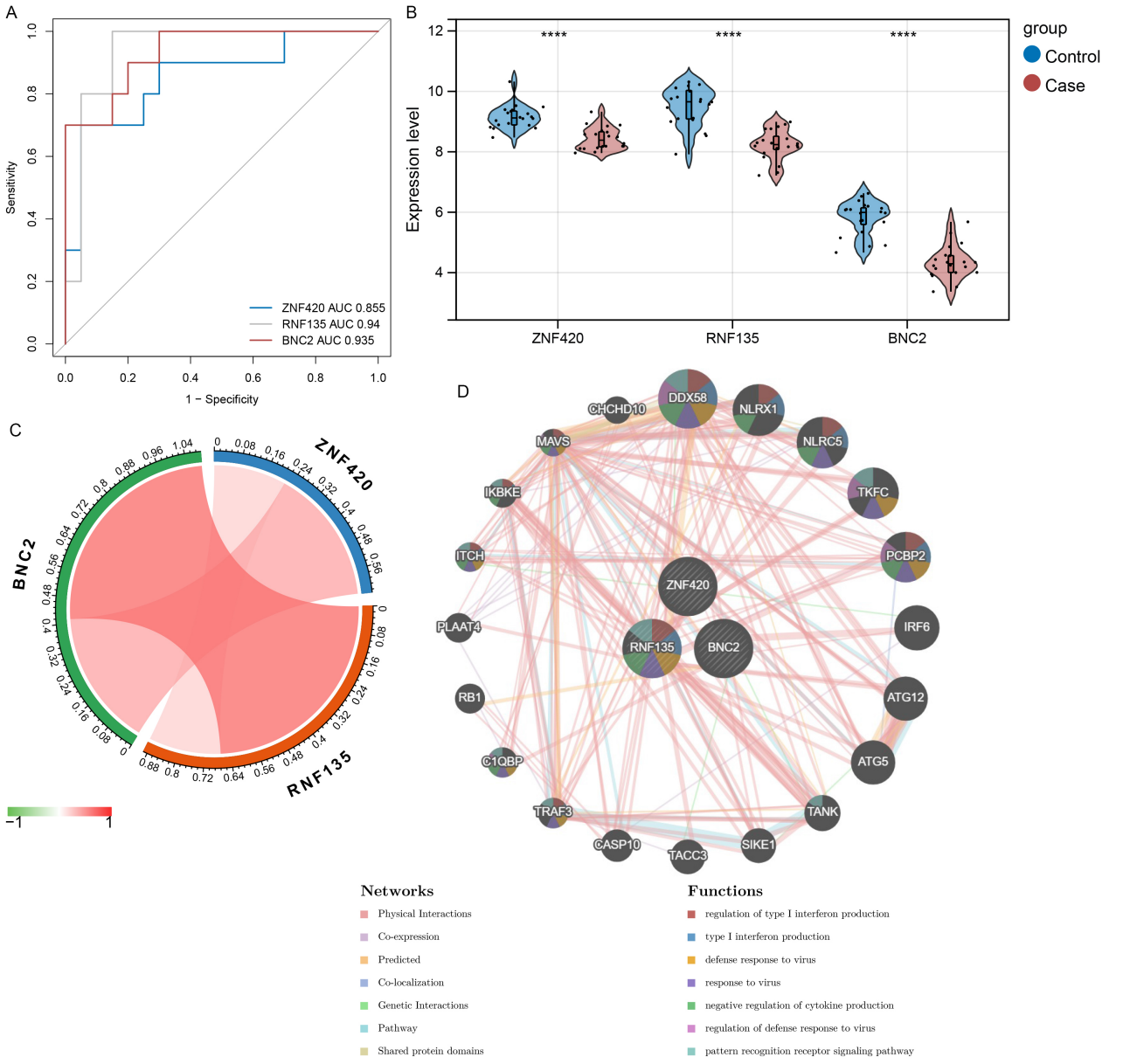

Fig. 5. Diagnostic value, correlation, and regulatory network analyses of biomarkers. (A) ROC analysis of three biomarkers. (B) The expression levels of 3 biomarkers between case and control groups. (C) Pearson correlation analysis among three biomarkers. (D) The interaction network of model genes predicted based on GeneMANIA database. "****" means $p < 0.0001$.

Discussion

OPCABG is a form of coronary artery bypass surgery with some advantages, particularly in decreasing postoperative complications and systemic inflammation, such as myocardial and brain damage [24]. Anesthesia during OPCABG reduces intraoperative blood loss and the need for intraoperative blood transfusion, thereby shortening the length of hospital stay. Importantly, anesthesia reduces inflammation, myocardial enzyme leakage, and myocardial reperfusion injury by exerting cardioprotective effects [25]. Anesthetic administration modulates gene expression to adapt to cardiac surgery in the human heart [1]. It is inferred that genes with differential expression induced by anesthetics during cardiovascular surgery may serve as clinically important cardiovascular biomarkers and help understand the mechanism underlying the protective effect of anesthetics on cardiac function. Thus, in the present study, we conducted an integrated bioinformatics analysis to explore cardiovascular biomarkers induced by anesthesia during OPCABG.

In this study, 24 *DE ZFPRGs* were identified based on 2274 ZFPRGs, 1102 common DEGs, and 1095 hub genes. Following machine learning, *ZNF420*, *RNF135*, and *BNC2* were selected as cardiovascular biomarkers. The diagnos-

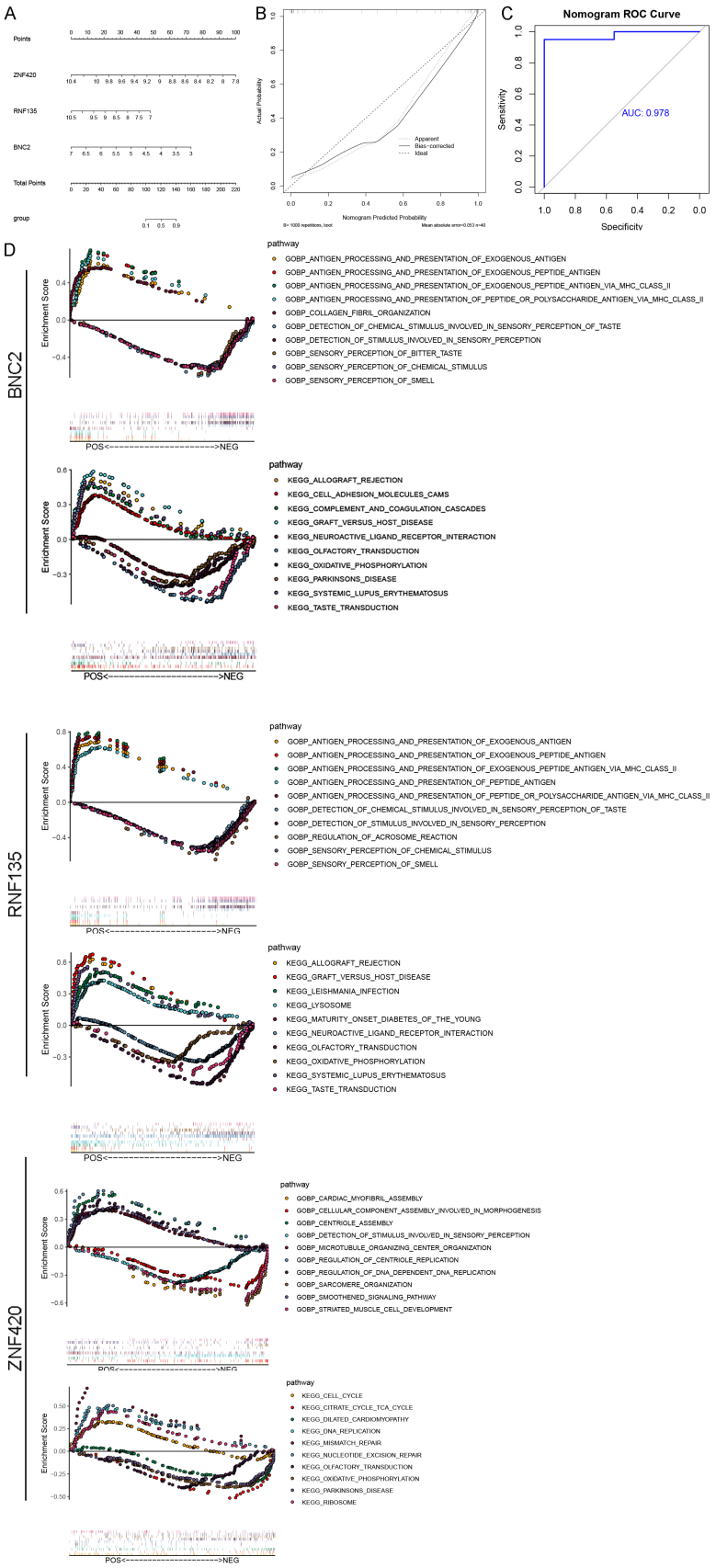

Fig. 6. Nomogram model construction and gene set enrichment analysis (GSEA) enrichment analysis. (A) nomogram model of three biomarkers. (B) Calibration curve. (C) ROC curve analysis of the nomogram model. (D) GSEA analysis of the single biomarker gene based on GO BP terms and Kyoto Encyclopedia of Genes and Genomes (KEGG) pathways.

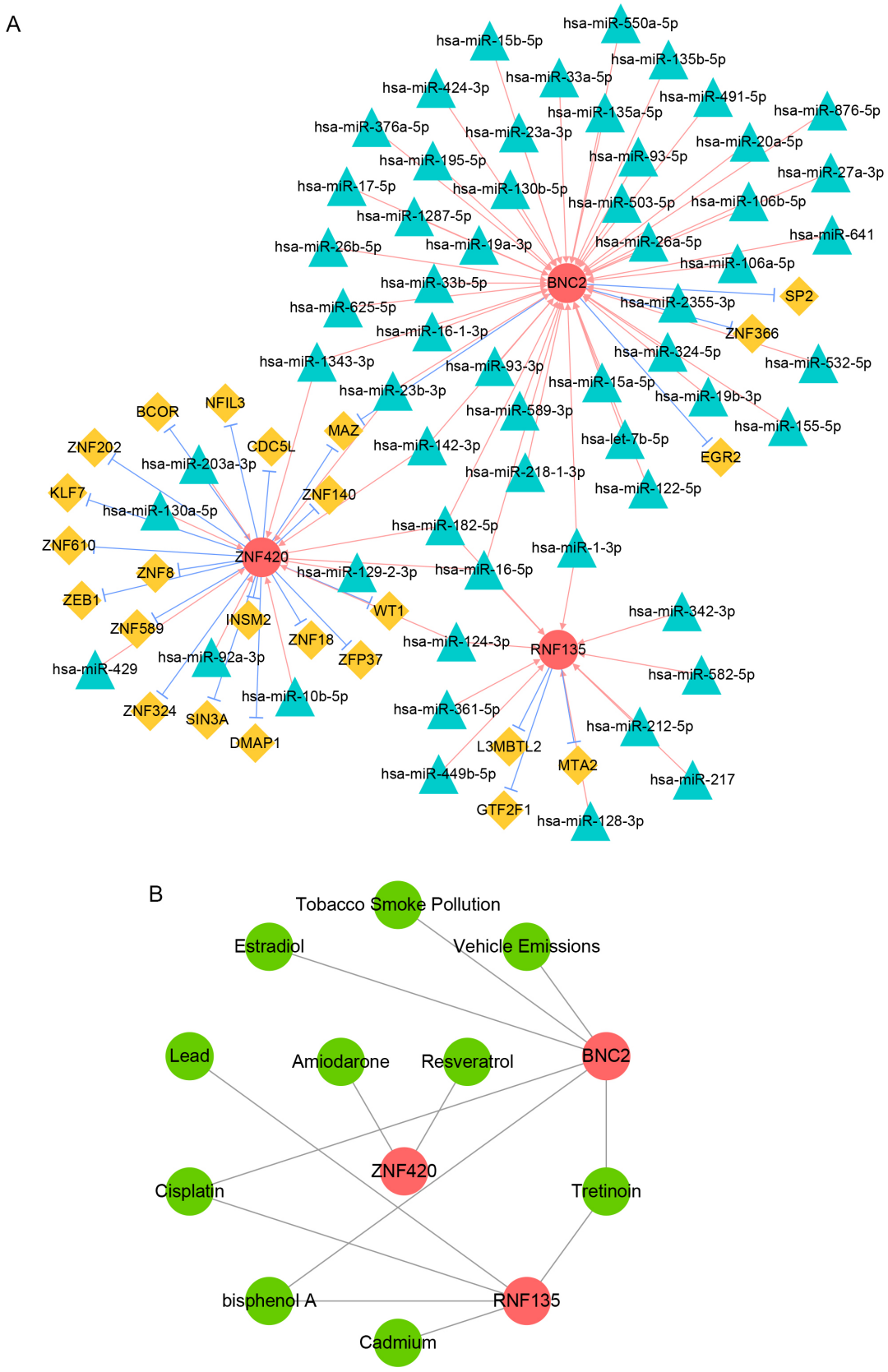

Fig. 7. MiRNA-mRNA-TF regulatory network construction and drug prediction of biomarkers. (A) microRNA (miRNA)-mRNA-TF (transcription factor) regulatory network constructed by 425 miRNA-mRNA-TF regulatory pairs. A red circle represents a biomarker, a yellow diamond represents a TF, and a cyan triangle represents a miRNA. (B) Drug-target regulatory network diagram.

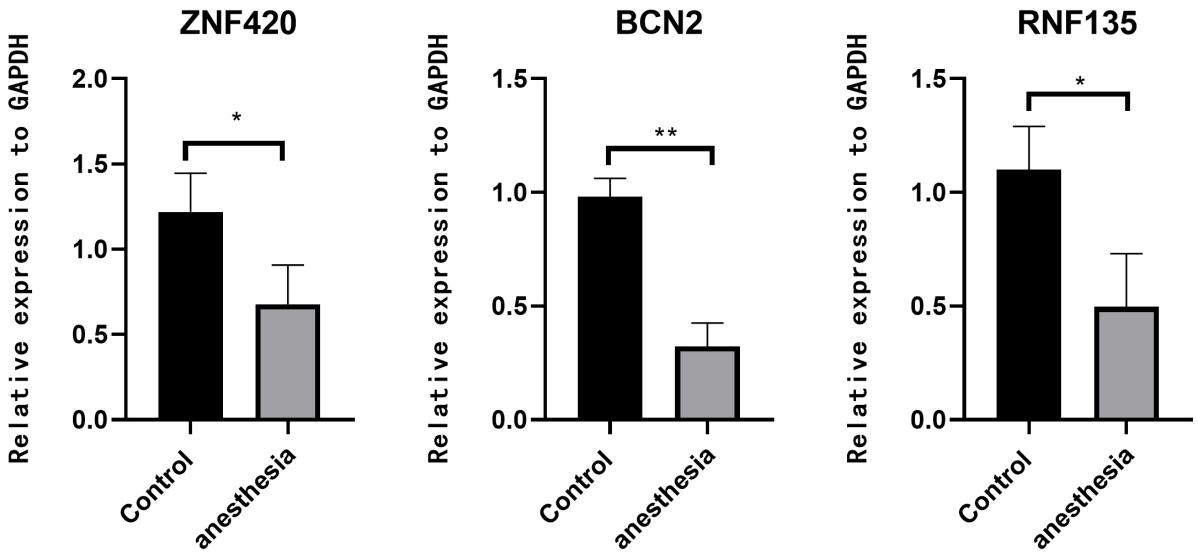

Fig. 8. Gene expression validation of biomarker genes in clinical samples. *$p < 0.05$, **$p < 0.01$.

tic value and accuracy of the three biomarkers were confirmed using ROC curves and nomogram models, suggesting that they were closely related to anesthesia-induced cardiac function. To the best of our knowledge, none of these three biomarkers have been reported to be associated with cardioprotection in previous studies, which indirectly embodies the research value of our study.

ZNF420, the human gene encoding Apak, negatively affects p53-mediated apoptosis [26]. P53-mediated signaling plays a key role in the apoptosis of cardiomyocytes induced by ischemia [27], reperfusion [28], and oxidative stress [29]. Cardiac surgery associated with ischemia-reperfusion injury triggers p53-mediated apoptosis of myocardial cells [29]. Our data suggested that *ZNF420* was expressed at significantly lower levels in cardiac tissues after cardiac surgery. We inferred that the overexpression of *ZNF420* could exert a protective role by suppressing myocardial apoptosis induced by ischemia-reperfusion [30]. GSEA revealed that *ZNF420* was associated with functions related to cardiac myofibril assembly and was involved in pathways of the TCA cycle. The TCA cycle is a central metabolic hub connecting multiple catabolic, anabolic, and anaplerotic reactions. TCA cycle-related metabolites are involved in a variety of physiological processes as epigenetic effectors and regulators of hypoxic responses [31]. In myocardial ischemia and cardiac injury, hypoxia severely alters the myocardial mitochondrial TCA cycle flux, reduces adenosine triphosphate (ATP) production, and leads to the intracellular accumulation of TCA cycle intermediates [31,32]. In addition, the TCA cycle is associated with the release of biosynthetic intermediates such as glucose, fatty acids, and non-essential amino acids. Fatty acids are the major fuel source in the heart under normoxic conditions, whereas glucose is converted into the basic fuel source during ischemia [33]. High levels of fatty acid oxidation increase the risk of postoperative contractile dysfunction [1]. Changes in plasma TCA cycle-related metabolites have been implicated in an increased risk of cardiovascular diseases or cardiac damage [34]. Although there is no evidence regarding the regulatory role of the TCA cycle, we speculate that *ZNF420* may be associated with cardioprotection in OPCABG by controlling myocardial energy metabolism. Interestingly, *RNF135* and *BNC2* were enriched in the oxidative phosphorylation pathway. The heart is the most energy-consuming organ in the body and requires high levels of mitochondrial oxidative phosphorylation [35], which is impaired in the heart under ischemia [36,37]. The TRIM-like gene *RNF135*, which encodes a RING finger protein, is the cause of neurofibromatosis and its function is unknown [38]. BNC2, a cell type-specific zinc finger protein, is related to color changes and the development of several types of cancer [39]. BNC2 is highly expressed in the fetal heart and penis [40] and is downregulated in myocardial ischemia models [41]. Although there is no direct evidence of the biological function of *RNF135* and *BNC2* in ischemic injury, both genes may exert cardioprotective effects induced by anesthesia by modulating oxidative phosphorylation in the heart under OPCABG.

To elucidate the regulatory mechanisms of these three biomarkers, we predicted their miRNAs and TFs and constructed a regulatory network. In this network, miR-182-5p and miR-16-5p simultaneously regulated the three biomarkers, suggesting that these two miRNAs may play critical regulatory roles. miR-182-5p is expressed at low levels in cardiomyocytes under hypoxia [42]. Treatment with miR-182 protects against myocardial ischemia/reperfusion injury by suppressing cell death [43]. MiR-16-5p is overexpressed in the plasma of patients with ischemic dilated cardiomyopathy. It also promotes endoplasmic reticulum

stress-induced inflammation and autophagy in human ventricular myocytes [44]. Recently, Toro *et al*. [45] demonstrated that suppressing miR-16-5p expression has the potential to protect the heart from endoplasmic reticulum- and oxidative stress-induced damage. Taken together, we speculate that *ZNF420*, *RNF135*, and *BNC2* may be involved in cardioprotection during OPCABG under the regulation of miR-182-5p and miR-16-5p.

This study has some limitations that cannot be ignored. First, this study was conducted using DNA microarray data, which may have limited the sensitivity, accuracy, and reproducibility of the results. Second, owing to a shortage of clinical samples, the protective effects of the biomarkers were not verified in clinical samples or cell lines. Thus, the cardioprotective effect of the biomarkers (*ZNF420*, *RNF135*, and *BNC2*) induced by anesthesia should be further investigated using cell lines and a large number of clinical samples.

Conclusion

In conclusion, our study identified three anesthesia-induced zinc finger proteins as cardioprotective biomarkers (*ZNF420*, *RNF135*, and *BNC2*) in OPCABG. The findings of this study may provide additional information on cardioprotection strategies in clinical surgery.

Abbreviations

DE, differentially expressed; DEGs, differentially expressed genes; GSEA, Gene Set Enrichment Analysis; OPCABG, off-pump coronary artery bypass grafting; PPI, protein-protein interaction; SVM, support vector machines; TF, transcription factor; WGCNA, Weighted gene co-expression network analysis; ZFPRGs, Zinc finger protein related genes.

Availability of Data and Materials

All data generated or analyzed during this study are included in this article. Further enquiries can be directed to the corresponding author.

Author Contributions

Both authors contributed to the study conception and design. Material preparation, data collection and analysis were performed by JH and JL. The first draft of the manuscript was written by JH and both authors commented on previous versions of the manuscript. Both authors contributed to editorial changes in the manuscript. Both authors read and approved the final manuscript. Both authors have participated sufficiently in the work to take public responsibility for appropriate portions of the content and agreed to be accountable for all aspects of the work in ensuring that questions related to its accuracy or integrity.

Ethics Approval and Consent to Participate

The study was performed in line with the principles of the Declaration of Helsinki. Approval was granted by the Ethics Committee of Weifang People's Hospital (No. 2023SDL360). And written informed consent was obtained from all individual participants included in the study.

Acknowledgment

Not applicable.

Funding

This research received no external funding.

Conflict of Interest

The authors declare no conflict of interest.

References

[1] Lucchinetti E, Hofer C, Bestmann L, Hersberger M, Feng J, Zhu M, *et al*. Gene regulatory control of myocardial energy metabolism predicts postoperative cardiac function in patients undergoing off-pump coronary artery bypass graft surgery: inhalational versus intravenous anesthetics. Anesthesiology. 2007; 106: 444–457.

[2] Mirhafez SR, Khadem SH, Sahebkar A, Movahedi A, Rahsepar AA, Mirzaie A, *et al*. Comparative effects of on-pump versus off-pump coronary artery bypass grafting surgery on serum cytokine and chemokine levels. IUBMB Life. 2021; 73: 1423–1431.

[3] Pawliszak W, Kowalewski M, Raffa GM, Malvindi PG, Kowalkowska ME, Szwed KA, *et al*. Cerebrovascular Events After No-Touch Off-Pump Coronary Artery Bypass Grafting, Conventional Side-Clamp Off-Pump Coronary Artery Bypass, and Proximal Anastomotic Devices: A Meta-Analysis. Journal of the American Heart Association. 2016; 5: e002802.

[4] Kusurin M, Majnaric M, Unic D, Baric D, Blazekovic R, Varvodic J, *et al*. Comparison between OPCABG and CABG Surgical Revascularization Using Transit Time Flow Measurement (TTFM). The Heart Surgery Forum. 2021; 2021: E963–E967.

[5] Rajakaruna C, Rogers C, Pike K, Alwair H, Cohen A, Tomkins S, *et al*. Superior haemodynamic stability during off-pump coronary surgery with thoracic epidural anaesthesia: results from a prospective randomized controlled trial. Interactive Cardiovascular and Thoracic Surgery. 2013; 16: 602–607.

[6] Dhurandhar V, Saxena A, Parikh R, Vallely MP, Wilson MK, Butcher JK, *et al*. Comparison of the Safety and Efficacy

of On-Pump (ONCAB) versus Off-Pump (OPCAB) Coronary Artery Bypass Graft Surgery in the Elderly: A Review of the ANZSCTS Database. Heart, Lung & Circulation. 2015; 24: 1225–1232.

[7] Pruna R, Artells R, Lundblad M, Maffulli N. Genetic biomarkers in non-contact muscle injuries in elite soccer players. Knee Surgery, Sports Traumatology, Arthroscopy: Official Journal of the ESSKA. 2017; 25: 3311–3318.

[8] Selvanayagam JB, Petersen SE, Francis JM, Robson MD, Kardos A, Neubauer S, *et al*. Effects of off-pump versus on-pump coronary surgery on reversible and irreversible myocardial injury: a randomized trial using cardiovascular magnetic resonance imaging and biochemical markers. Circulation. 2004; 109: 345–350.

[9] Zhao H, Wang W, Liu L, Wang J, Yan Q. Functional Modular Network Identifies the Key Genes of Preoperative Inhalation Anesthesia and Intravenous Anesthesia in Off-Pump Coronary Artery Bypass Grafting. Computational and Mathematical Methods in Medicine. 2020; 2020: 4574792.

[10] Likhvantsev VV, Landoni G, Levikov DI, Grebenchikov OA, Skripkin YV, Cherpakov RA. Sevoflurane Versus Total Intravenous Anesthesia for Isolated Coronary Artery Bypass Surgery With Cardiopulmonary Bypass: A Randomized Trial. Journal of Cardiothoracic and Vascular Anesthesia. 2016; 30: 1221–1227.

[11] Pasin L, Landoni G, Cabrini L, Borghi G, Taddeo D, Saleh O, *et al*. Propofol and survival: a meta-analysis of randomized clinical trials. Acta Anaesthesiologica Scandinavica. 2015; 59: 17–24.

[12] Huang Z, Zhong X, Irwin MG, Ji S, Wong GT, Liu Y, *et al*. Synergy of isoflurane preconditioning and propofol postconditioning reduces myocardial reperfusion injury in patients. Clinical Science (London, England: 1979). 2011; 121: 57–69.

[13] Lin S, Neelankavil J, Wang Y. Cardioprotective Effect of Anesthetics: Translating Science to Practice. Journal of Cardiothoracic and Vascular Anesthesia. 2021; 35: 730–740.

[14] De Hert SG, Van der Linden PJ, Cromheecke S, Meeus R, Nelis A, Van Reeth V, *et al*. Cardioprotective properties of sevoflurane in patients undergoing coronary surgery with cardiopulmonary bypass are related to the modalities of its administration. Anesthesiology. 2004; 101: 299–310.

[15] Cassandri M, Smirnov A, Novelli F, Pitolli C, Agostini M, Malewicz M, *et al*. Zinc-finger proteins in health and disease. Cell Death Discovery. 2017; 3: 17071.

[16] Ozyildirim S, Baltaci SB. Cardiovascular Diseases and Zinc. Biological Trace Element Research. 2023; 201: 1615–1626.

[17] Li F, Yang Y, Xue C, Tan M, Xu L, Gao J, *et al*. Zinc Finger Protein ZBTB20 protects against cardiac remodelling post-myocardial infarction via ROS-TNFα/ASK1/JNK pathway regulation. Journal of Cellular and Molecular Medicine. 2020; 24: 13383–13396.

[18] Meng XY, Yu HL, Zhang WC, Wang TH, Mai X, Liu HT, *et al*. ZFP580, a novel zinc-finger transcription factor, is involved in cardioprotection of intermittent high-altitude hypoxia against myocardial ischemia-reperfusion injury. PLoS ONE. 2014; 9: e94635.

[19] Langfelder P, Horvath S. WGCNA: an R package for weighted correlation network analysis. BMC Bioinformatics. 2008; 9: 559.

[20] Yu G, Wang LG, Han Y, He QY. clusterProfiler: an R package for comparing biological themes among gene clusters. Omics: a Journal of Integrative Biology. 2012; 16: 284–287.

[21] Yuan GX, Ho CH, Lin CJ. An improved glmnet for l1-regularized logistic regression. Journal of Machine Learning Research. 2012; 13: 1999–2030.

[22] Meyer D, Dimitriadou E, Hornik K, Weingessel A, Leisch F, Chang C, *et al*. e1071: Misc functions of the Department of Statistics (e1071), TU Wien. R Package Version. 2014; 1: 9.

[23] Levinson N. The Wiener (root mean square) error criterion in filter design and prediction. Journal of Mathematics and Physics. 1946; 25: 261–278.

[24] Bhaskaran K, Arumugam G, Vinay Kumar PV. A prospective, randomized, comparison study on effect of perioperative use of chloride liberal intravenous fluids versus chloride restricted intravenous fluids on postoperative acute kidney injury in patients undergoing off-pump coronary artery bypass grafting surgeries. Annals of Cardiac Anaesthesia. 2018; 21: 413–418.

[25] Brown JM, Poston RS, Gammie JS, Cardarelli MG, Schwartz K, Sikora JAH, *et al*. Off-pump versus on-pump coronary artery bypass grafting in consecutive patients: decision-making algorithm and outcomes. The Annals of Thoracic Surgery. 2006; 81: 555–561.

[26] Tian C, Xing G, Xie P, Lu K, Nie J, Wang J, *et al*. KRAB-type zinc-finger protein Apak specifically regulates p53-dependent apoptosis. Nature Cell Biology. 2009; 11: 580–591.

[27] Sato M, Jiao Q, Honda T, Kurotani R, Toyota E, Okumura S, *et al*. Activator of G protein signaling 8 (AGS8) is required for hypoxia-induced apoptosis of cardiomyocytes: role of G betagamma and connexin 43 (CX43). The Journal of Biological Chemistry. 2009; 284: 31431–31440.

[28] Kang PM, Haunstetter A, Aoki H, Usheva A, Izumo S. Morphological and molecular characterization of adult cardiomyocyte apoptosis during hypoxia and reoxygenation. Circulation Research. 2000; 87: 118–125.

[29] von Harsdorf R, Li PF, Dietz R. Signaling pathways in reactive oxygen species-induced cardiomyocyte apoptosis. Circulation. 1999; 99: 2934–2941.

[30] Owen OE, Kalhan SC, Hanson RW. The key role of anaplerosis and cataplerosis for citric acid cycle function. The Journal of Biological Chemistry. 2002; 277: 30409–30412.

[31] Martínez-Reyes I, Chandel NS. Mitochondrial TCA cycle metabolites control physiology and disease. Nature Communications. 2020; 11: 102.

[32] Müller OJ, Heckmann MB, Ding L, Rapti K, Rangrez AY, Gerken T, *et al*. Comprehensive plasma and tissue profiling reveals systemic metabolic alterations in cardiac hypertrophy and failure. Cardiovascular Research. 2019; 115: 1296–1305.

[33] Stanley WC, Recchia FA, Lopaschuk GD. Myocardial substrate metabolism in the normal and failing heart. Physiological Reviews. 2005; 85: 1093–1129.

[34] Santos JL, Ruiz-Canela M, Razquin C, Clish CB, Guasch-Ferré M, Babio N, *et al*. Circulating citric acid cycle metabolites and risk of cardiovascular disease in the PREDIMED study. Nutrition, Metabolism, and Cardiovascular Diseases: NMCD. 2023; 33: 835–843.

[35] Pohjoismäki JL, Goffart S. The role of mitochondria in cardiac development and protection. Free Radical Biology & Medicine. 2017; 106: 345–354.

[36] Piper HM, Noll T, Siegmund B. Mitochondrial function in the oxygen depleted and reoxygenated myocardial cell. Cardiovascular Research. 1994; 28: 1–15.

[37] Solaini G, Harris DA. Biochemical dysfunction in heart mitochondria exposed to ischaemia and reperfusion. The Biochemical Journal. 2005; 390: 377–394.

[38] Oshiumi H, Matsumoto M, Hatakeyama S, Seya T. Riplet/RNF135, a RING finger protein, ubiquitinates RIG-I to promote interferon-beta induction during the early phase of viral infection. The Journal of Biological Chemistry. 2009; 284: 807–817.

[39] Wu Y, Zhang X, Liu Y, Lu F, Chen X. Decreased Expression of BNC1 and BNC2 Is Associated with Genetic or Epigenetic Regulation in Hepatocellular Carcinoma. International Journal of Molecular Sciences. 2016; 17: 153.

[40] Vanhoutteghem A, Messiaen S, Hervé F, Delhomme B, Moi-

son D, Petit JM, *et al*. The zinc-finger protein basonuclin 2 is required for proper mitotic arrest, prevention of premature meiotic initiation and meiotic progression in mouse male germ cells. Development. 2014; 141: 4298–4310.

[41] Xu Y, Lv X, Cai R, Ren Y, He S, Zhang W, *et al*. Possible implication of miR-142-3p in coronary microembolization induced myocardial injury via ATXN1L/HDAC3/NOL3 axis. Journal of Molecular Medicine (Berlin, Germany). 2022; 100: 763–780.

[42] Zhang X, Xiao C, Liu H. Ganoderic Acid A Protects Rat H9c2 Cardiomyocytes from Hypoxia-Induced Injury via Up-Regulating miR-182-5p. Cellular Physiology and Biochemistry: International Journal of Experimental Cellular Physiology, Biochemistry, and Pharmacology. 2018; 50: 2086–2096.

[43] Lee SY, Lee S, Choi E, Ham O, Lee CY, Lee J, *et al*. Small molecule-mediated up-regulation of microRNA targeting a key cell death modulator BNIP3 improves cardiac function following ischemic injury. Scientific Reports. 2016; 6: 23472.

[44] Calderon-Dominguez M, Mangas A, Belmonte T, Quezada-Feijoo M, Ramos M, Toro R. Ischemic dilated cardiomyopathy pathophysiology through microRNA-16-5p. Revista Espanola De Cardiologia (English Ed.). 2021; 74: 740–749.

[45] Toro R, Pérez-Serra A, Mangas A, Campuzano O, Sarquella-Brugada G, Quezada-Feijoo M, *et al*. miR-16-5p Suppression Protects Human Cardiomyocytes against Endoplasmic Reticulum and Oxidative Stress-Induced Injury. International Journal of Molecular Sciences. 2022; 23: 1036.